Mon. Not. R. Astron. Soc. **000**, 1–?? (2013) Printed 4 February 2014 (MN LATEX style file v2.2)

Pressure-driven fragmentation of multi-phase clouds at high redshift

H. Dhanoa[1⋆], J. Mackey[2], and J. Yates[1]
[1] *Department of Physics and Astronomy, University College London, Gower Street, London, WC1E 6BT*
[2] *Argelander-Institut für Astronomie, Auf dem Hügel 71, Bonn D-53121, Germany*

4 February 2014

ABSTRACT
The discovery of a hyper metal-poor star with total metallicity of $\leqslant 10^{-5}$ $Z_{\odot}$, has motivated new investigations of how such objects objects can form from primordial gas polluted by a single supernova. In this paper, we present a shock-cloud model, which simulates a supernova remnant interacting with a cloud in a metal-free environment at redshift $z = 10$. We consider pre-supernova conditions which include a multiphase neutral medium and H II region. We model a small dense clump ($n = 100$ cm^{-3} s), located 40 pc from a 40 $M_{\odot}$ metal-free star, embedded in a $n = 10$ cm^{-3} ambient cloud. We follow the evolution of the supernova remnant (explosion energy 10^{52} erg) and its subsequent interaction with the dense clump. This is the first study to include a comprehensive treatment of non-equilibrium chemistry and associated radiative cooling processes occurring at all stages of a shock-cloud model. We have included a primordial chemistry network that covers the temperature range $10 - 10^{9}$ K, which is coupled to thermal models of atomic and molecular cooling and heating. We find a 10^{3} density enhancement of the clump (i.e maximum density ~ 78000 cm^{-3}) within this metal-free model. This is consistent with Galactic shock-cloud models considering solar metallicity gas with equilibrium cooling functions. Despite this strong compression, the cloud does not become gravitationally unstable. We find that the small cloud modelled here is destroyed for shock velocities $\gtrsim 50$ km s^{-1}, and not significantly affected by shocks with velocity $\lesssim 30$ km s^{-1}. Rather specific conditions are required to make such a cloud collapse.

Key words: High redshift - stars: formation - supernovae: general - molecules

1 INTRODUCTION

The first galaxies are thought to form around redshift $z \geqslant 10$ when the universe was less than 500 Myrs old. These nascent environments are considered to be the key sites where the transition from Population III to Population II stars took place. A possible fossil from this era is SDSS J102915+172927, which is a low-mass ($M < 0.8\ M_{\odot}$) star with a total metallicity of $Z < 10^{-5}\ Z_{\odot}$ (Caffau et al. 2011). As a result of such low metallicity, it is deduced that the star formed from primordial gas which was polluted by a single supernova. This star has challenged the theory that a critical metallicity is needed to form sub-solar-mass Population II star (Klessen et al. 2012). A better understanding of the role of star formation and its feedback effects at high redshifts is extremely important in relation to the formation of such objects.

Here we investigate cloud-shock interactions in a metal-free environment, as this has not been investigated in previous work. Radiative cooling is the critical factor in promoting hydrodynamic and gravitational instabilities. Hence in this paper we focus on the non-equilibrium cooling that dominates this system. This can only be captured correctly by including non-equilibrium chemistry (linked to a thermal model) for the full temperature range associated with a supernova shock model. Kitayama & Yoshida (2005) and Vasiliev et al. (2008) highlighted the important link between the radial distribution of primordial gas prior to the supernova explosion and the subsequent evolution of the supernova remnant and the formation of extremely metal-poor stars. Therefore we include both the H II region and neutral medium, to obtain a realistic supernova shell evolution. Once the supernova shock begins to travel within neutral matter, it interacts with a multi-phase medium, which cannot be characterised by a single density. The pressure driven compression and fragmentation of dense neutral clumps found in this neutral matter could be possible site for low-mass star formation.

At present most supernova shock models for the early universe couple chemical and thermal evolution for temperatures below 10^{4} K and focus on the fragmentation of the supernova shell itself. Machida et al. (2005) were the first to investigate primordial low-mass star formation at high redshift via this method. The authors included non-equilibrium cooling from H_2 and HD molecules, coupled to a semi-analytic dynamic model. They found that shell fragmentation was possible for explosion energies $\geqslant 10^{51}$ erg and ambient density $n > 3$ cm^{-3}. The contraction of the fragments was studied, and they found the Jeans mass reduced to $\sim$1 $M_{\odot}$. Nagakura et al. (2009) extended the model to include metal line cooling for low-metallicity gas coupled to a 1D hydrodynamic code. They use linear perturbation analysis of the expanding shell to con-

⋆ E-mail: hd@star.ucl.ac.uk (HD); jmackey@astro.uni-bonn.de (JM)

strain the criteria for fragmentation and found that there is little dependency on metallicity in the range $10^{-4} - 10^{-2}\,Z_{\odot}$. Compared to Machida et al. (2005), they found that fragmentation only occurred in higher ambient uniform densities ($n \geqslant 100$ cm^{-3} for a 10^{51} erg explosion and $n \geqslant 10$ cm^{-3} for a 10^{52} erg explosion), resulting in fragments of mass $10^2 - 10^3$ M$_{\odot}$.

Chiaki et al. (2013) developed a 1D supernova model that considers 10^{-5} Z$_{\odot}$ metallicity gas. The authors include metal-free non-equilibrium chemistry for temperatures below 10^4 K, with separate calculated rates for metal-line cooling. However, above 10^4 K the authors utilise the collisional ionisation equilibrium cooling function by Sutherland & Dopita (1993). Supernova shells are expected to become gravitationally unstable for a wide range of explosion energies ($10^{51} - 3 \times 10^{52}$ erg) and ambient uniform densities ($n \geqslant 10$ cm^{-3}). The thermal evolution of a shell fragment was followed using a one-zone model which includes low-metallicity chemistry and dust cooling. They expect the fragment to evolve into a high density core (10^{13} cm^{-3}), which will evetually form multiple clumps of mass $0.01 - 0.1$ M$_{\odot}$.

Also using a one-zone model, Mackey et al. (2003) modelled an equilibrium primordial gas cloud that is shocked by a supernova. The shocked cloud is heated to a higher entropy state and it is assumed to cool isobarically back to its original equilibrium temperature, but now at a much higher density than before. In this way the Jeans mass of the gas could be reduced by a large factor, allowing much lower-mass stars to form. This argument also applies to smooth ISM distributions, as discussed above (Machida et al. 2005; Nagakura et al. 2009; Chiaki et al. 2013), as long as isobaric conditions hold in the decelerating shell. The one-zone model of Mackey et al. (2003) also crucially depends on the isobaric assumption to increase the gas density in the cooling cloud.

In reality, however, pressure is a decreasing function of time in a supernova remnant, because the explosion is (by definition) vastly over-pressured compared to its surroundings. As long as the expansion timescale of the supernova $t_{\rm exp} = R_{\rm sh}/\dot{R_{\rm sh}}$ (where $R_{\rm sh}$ is the shock radius and $\dot{R_{\rm sh}}$ its velocity) is short compared to the local timescale for gravitational effects (i.e the free-fall time $t_{\rm ff} = 1/\sqrt{G\rho}$, where ρ is the gas density and G the gravitational constant) then the time-dependence of the external pressure is an important part of the solution. The passage of a strong shock through a dense cloud can also have catastrophic consequences for the cloud (Klein et al. 1994) through turbulent hydrodynamic instabilities. Both of these considerations are best addressed with multi-dimensional hydrodynamic simulations, cannot be captured in one-zone models.

Star formation triggered by the interaction between supernova explosions and molecular clouds (radius $\geqslant$ 5pc) has been investigated in the Galactic environment by Melioli et al. (2006). Using an analytic study based on comparing the gravitational free-fall time and destruction time scale of the cloud, (which depends on a number of parameters including radiative cooling), the authors constrain where cloud collapse (and therefore possible star formation) can occur in the supernova remnant radius vs. cloud density parameter space. By running a suite of 3D hydrodynamic simulations, they were able to confirm that these numerical models were consistent with their analytic constraints. This work was extended by Leão et al. (2009) to include magnetic fields and found their results still are consistent with analytic results. Both authors recognise that using an approximate polytropic pressure equation to represent radiative cooling maybe an over simplification and more realistic cooling functions are required.

Johansson & Ziegler (2013) have concentrated on the compression of smaller clouds (radius $\sim$ 1 pc) found in the Galactic interstellar medium as a method of triggered star formation. Their MHD simulations (without self-gravity) concentrate on the radiative interaction between the shock and the cloud. The cooling function utilised is a peiceweise power-law given by Sánchez-Salcedo et al. (2002) and Slyz et al. (2005), and assumes collisional ionisation equilibrium. They find that the cloud fragments into small dense cool clumps but they do not become Jeans unstable. Importantly they find that initial density enhancements within the cloud can increase by a factor of $10^3 - 10^5$, which eventually relaxes to a final density enhancement of $10^2 - 10^3$. This is consistent with results by Vaidya et al. (2013), who have a similar model which includes self gravity. They find that gravity does not contribute to the large increase in density but plays an important role by preventing the re-expansion of the high density region.

These studies have highlighted that radiative cooling is a crucial process in the interaction between shocks and clouds. Therefore it is very important to include the non-equilibrium cooling that dominates this process, which cannot be captured using cooling functions that assume equilibrium abundances of their coolants. In this paper we present a model which includes the non-equilibrium metal-free chemistry and its associated cooling for the evolution of a supernova remnant and its subsequent interaction of a small dense clump embedded in a neutral cloud at redshift $z = 10$. In section §2 we outline how the initial conditions are generated by the pre-supernova model, and introduce the chemo-dynamic modelling of the supernova remnant. The results describing the generation of the pre-supernova model, the 1D Supernova model and the 2D interaction of the clump and shock, are presented in section §3. Finally, in sections §4 and §5 we discuss our findings and give a summary of the conclusions.

2 METHODS AND INITIAL CONDITIONS

We have modelled the interaction of a supernova shell with a dense clump in three stages:

(i) the pre-supernova phase, where the dynamical effects of photoionization heating from the star are modelled;
(ii) the post-supernova phase, where the supernova blast wave expands into the relic H II region left by the star; and
(iii) the shock-cloud interaction, where the expanding supernova shell compresses a dense cloud.

The first two stages are simulated in one dimension with spherical symmetry, whereas the third stage is simulated in two dimensions with rotational symmetry. This is because compression and fragmentation of the clump cannot be captured within 1D models. However, it is possible to achieve a good representation of the evolution of the supernova remnant in 1D models, assuming that the shell has not interacted with any dense clumps (Jun et al. 1996).

2.1 Pre-supernova phase

We use the radiation-magnetohydrodynamics code PION (Mackey & Lim 2010, 2011) for the simulations presented here, first in one dimension (1D) with spherical symmetry and later in two dimensions (2D) with rotational (axi-)symmetry. PION uses an explicit, finite-volume, integration scheme that is accurate to second order in time and space (Falle 1991). Here only the Euler equations of hydrodynamics are solved (i.e. magnetic fields are not considered), together with the ionisation rate equation of hydrogen and associated

non-equilibrium heating and cooling processes. The microphysical processes of ionisation, recombination, heating and cooling are coupled to hydrodynamics using Algorithm 3 in Mackey (2012).

We consider a metal-free star exploding in a small galaxy at redshift $z = 10$, sweeping up the ambient medium to form an expanding shell. The simplified initial condition consists of a uniform neutral ISM with hydrogen number density $n = 10\,\mathrm{cm}^{-3}$. Into this we place a dense cloud with (uniform) number density $n = 100\,\mathrm{cm}^{-3}$, radius $r_\mathrm{c} = 1.3\,\mathrm{pc}$, and located at $r = 40\,\mathrm{pc}$ from the star (which is at the origin). The gas is comprised of atomic hydrogen and helium (number density ratio of 1.00:0.08) and is cooled via atomic processes. We assume the star has formed in a sufficiently large galaxy that gravitational potential gradients can be neglected in the hydrodynamical evolution of the system. This is the simplest possible model for feedback from the massive star to a nearby cloud.

For the star's properties we take the 40 $\mathrm{M}_\odot$ metal-free model from Schaerer (2002) with no mass loss. This has a lifetime of 3.86 Myr, an effective temperature $T_\mathrm{eff} = 10^{4.9}\,\mathrm{K}$, and a time-averaged H-ionising photon luminosity $Q_0 = 2.47 \times 10^{49}\,\mathrm{s}^{-1}$. For simplicity we distribute these photons according to a blackbody spectrum with the star's T_eff. We ignore any post main sequence evolutionary effects because this comprises a small fraction of the star's life, and because the evolution is very uncertain. This model in Schaerer (2002) also remains relatively blue for its full lifetime, thus supporting our approximation of excluding a red giant phase.

2.2 Supernova Remnant phase

A supernova remnant is dominated by non-equilibrium cooling, therefore we developed a microphysics module which links the non-equilibrium chemistry and its associated cooling. This was accomplished by solving the following set of equations:

$$\frac{\partial E}{\partial t} = -\Lambda(\Sigma x_m, \rho, \mathrm{T}) + \Gamma(\Sigma x_n, \rho, \mathrm{T}) \quad (1)$$

$$\frac{\partial x_i}{\partial t} = C_i\left(x_j, \rho, \mathrm{T}\right) - D_i\left(x_j, \rho, \mathrm{T}\right) x_i \quad (2)$$

where E is the internal energy density (in erg cm^{-3}), Λ is the cooling function of the gas (in erg $\mathrm{cm}^{-3}\,\mathrm{s}^{-1}$), Γ is the heating function of the gas (in erg $\mathrm{cm}^{-3}\,\mathrm{s}^{-1}$), x_i is the fractional abundance of a chemical species, i, for a total number of chemical species N_s, T is the temperature of the gas (K), ρ is the total mass density of the gas (g cm^{-3}), C is the formation rate of the species and D is the destruction rate of the species. We use a chemical network of 11 species (H, He, H_2, H^+, H_2^+, H_3^+, HeH^+, He^+, He^{++}, H^- and e^-) and 42 reactions. The chemical rates cover the temperature range $10 - 10^9$ K, which are described in appendix B. The atomic species and electron fraction are treated numerically as conservation equations.

The supernova is modelled by injecting thermal energy, not kinetic (i.e. we ignore the free-expansion phase). Therefore at very early times the newly shocked gas has an artificially high temperature (T$> 10^9$ K), and at these temperatures we utilise the value of the reaction rates at 10^9 K. To avoid artificial overcooling at early times, we only switch on the cooling when the gas adiabatically cooled down to 10^8 K. The thermal model includes atomic cooling (Fukugita & Kawasaki 1994; Hummer 1994), Bremmstrahlung cooling (Hummer 1994; Shapiro & Kang 1987), inverse Compton scattering (Peebles 1971) and molecular line cooling from H_2, H_2^+ and H_3^+ (Glover & Abel 2008; Hollenbach & McKee 1979; Glover & Savin 2009). The heating processes included in the model are CMB heating (assumed equal to $\Lambda(\mathrm{T_{CMB}})$) and cosmic ray heating (Glover & Jappsen 2007). We set the cosmic ray ionisation rate at $\zeta = 10^{-18}\,\mathrm{s}^{-1}$ assuming the supernova remnant to be their source. Further discussion of parameters and full details of the chemical model will be presented in a forthcoming paper. The chemical and dynamic tests for our model are presented in the appendices.

Parameters	
Shell thickness	0.08 pc
Maximum shell density	1976 cm^{-3}
Minimum shell temperature	920 K
Shell velocity	39 km s^{-1}
Clump radius	1.3 pc
Maximum clump density	104 cm^{-3}
Minimum clump temperature	872 K

Table 1. Initial conditions of 2D model

3 RESULTS

3.1 Pre-supernova phase

The radial profile of the initial conditions and the pre-supernova ISM are plotted in Fig. (1). The gas density inside the photoionised H II region ($r < 33\,\mathrm{pc}$) has decreased compared to the initial conditions (to close to $n = 1\,\mathrm{cm}^{-3}$) because photoheating has driven its expansion. In this model we only include atomic cooling, we assume that the H_2 within the gas has been destroyed as a result of Lyman-Werner radiation from the star. The shocked neutral ISM has only weak atomic coolants and so has not formed a shell, and remains very close to the initial ISM density. The cloud (or in 1D a shell) has been pushed outwards by the H II region expansion, and is moving out at $v \approx 2\,\mathrm{km\,s}^{-1}$ (Fig. 1b). The wave reflected back inwards is driving the negative velocity seen between $16 < r < 30\,\mathrm{pc}$, and this is a transient feature imposed by the assumed spherical symmetry (which forces waves to reflect back and forth between the origin and any strong discontinuities). It has little effect on the overall solution except to marginally increase the density in this radius range. The temperature profile of the H II region is typical of that produced by hot stars in metal-free gas (Iliev et al. 2006).

3.2 Supernova Remnant phase

The output from the pre-supernova model is utilised as the initial conditions of the 1D supernova model. The clump has been moved to 45 pc due to the weak shock driven by dynamical expansion of the H II region (Figure 1a). When mapping the chemical species, we assume the percentage of ionised hydrogen and helium (He^+) are equal, and the initial molecular fractions are set to zero. A 10^{52} erg explosion is initiated and a shell starts to form at $\sim$27 pc. After 0.2012 Myr the supernova shock is well into the radiative phase, so a thin shell has formed that is about 200$\times$ denser than the pre-shock gas. This agrees well with the isothermal shock jump conditions, where the overdensity is equal to the Mach number ($\mathcal{M}$) squared. In the shell, the isothermal sound speed is $a \approx 2.5\,\mathrm{km\,s}^{-1}$, so $\mathcal{M}^2 \approx (39/2.5)^2 \approx 240$. This is also similar to the maximum overdensity obtained from the test calculation in Appendix A. In the interior of the supernova remnant the usual Sedov-Taylor solution remains imprinted on the fluid quantities: the

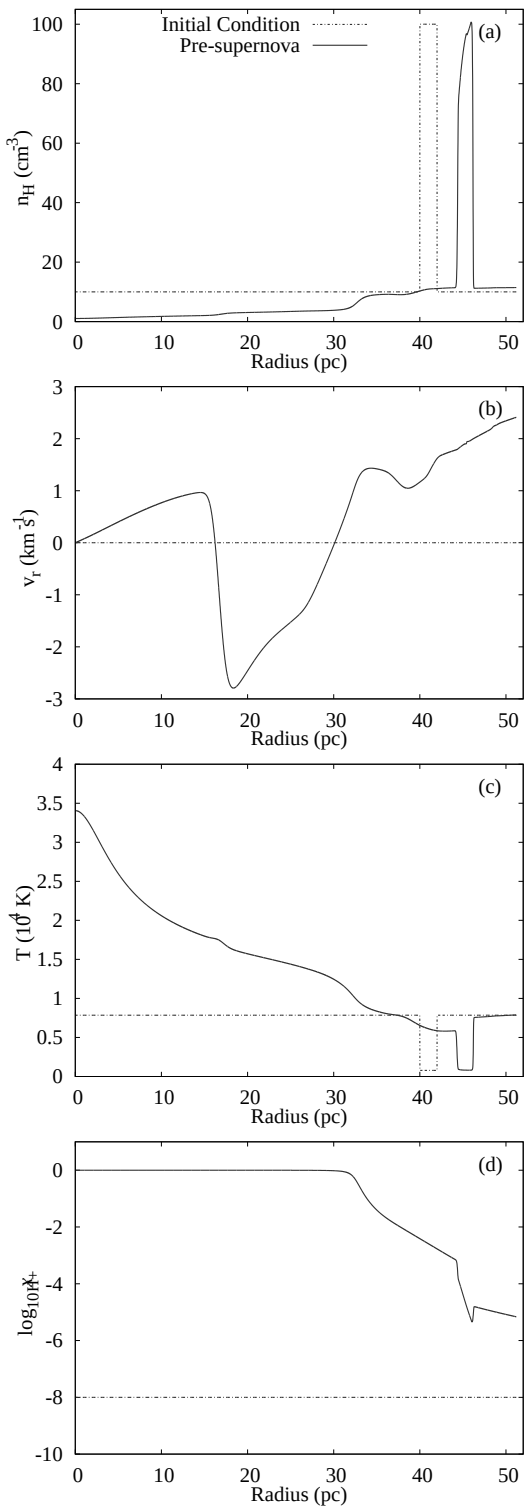

Figure 1. Plots of gas number density (a), velocity (b), temperature (c), and H^+ fraction (d) as a function of distance from the star. The dashed lines show the initial conditions and the solid lines the conditions at the pre-supernova stage.

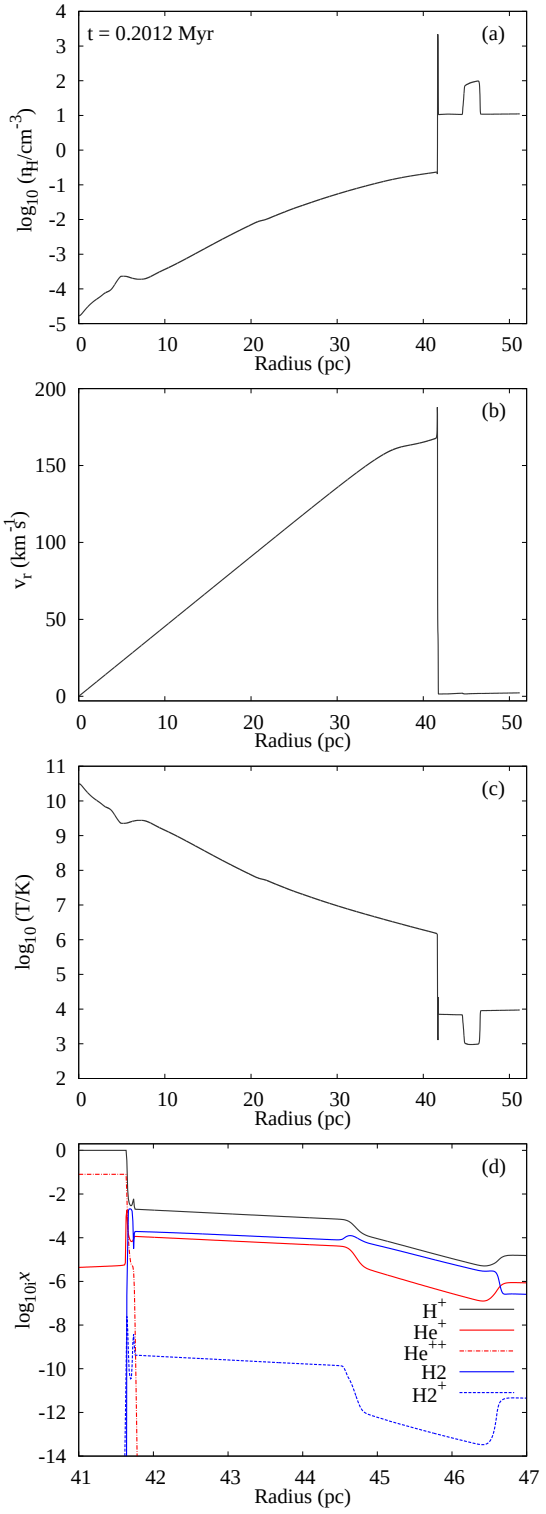

Figure 2. Gas number density (a), expansion velocity (b), temperature (c), and species fractions (d) as a function of distance from the star for the 1D post-supernova evolution, at $t = 0.2012$ Myr after the supernova explosion. Note that panel (d) has a different x-axis to the other panels, zoomed in to show only the chemistry of the supernova shell and the overdense cloud (smaller and larger radii show little variation). The supernova shell is at $r \approx 41.7$ pc, and the overdense cloud at $r \approx 44.6 - 46.6$ pc.

density and velocity tend to zero at the origin, and the temperature increases to maintain the constant interior pressure. The molecular fractions are all negligible in the hot interior, and have a maximum in the shocked shell because here the density is highest but there is also still a non-negligible electron fraction from heating in the shell's forward shock. The maximum H_2 fraction in the shell is $x(H_2) \approx 0.002$, in agreement with previous work (Machida et al. 2005).

The 1D supernova model is terminated when the shell reaches 41.9 pc (before it collides with the clump) and the output of this simulation (Figure 2) is mapped onto a 2D axisymmetric grid (7.68 pc $\times$ 3.2 pc). The initial conditions for the 2D model are outlined in Table 1. The supernova shell is already travelling within the neutral ambient cloud and is proceeding towards a dense spherical clump ($\sim$ 19 $M_\odot$) at a velocity of 39 km s^{-1}. The clump centre is 46 pc from the progenitor star. Figure 3 displays the evolution of the clump as the supernova shell collides and compresses it. The upper half plane of the plots display the log of the number density ($\log_{10}$ n_H/cm^{-3}) and corresponding lower plane represents the reflected axisymmetric simulation displaying the log of the temperature. The legend at the top left shows the fractional abundance of H_2 for each of the four abundance contours. The numbers represent 20%, 40%, 60%, and 80% of the maximum H_2 fraction in the simulation.

After 0.31 Myr the shock has passed through half of the clump (upper plot in Figure 3), we can see from Figure 4 the maximum density of clump is $\sim$ 6000 cm^{-3}. After 0.41 Myrs the supernova shell has passed through the clump completely (middle plot in Figure 3), and due to the decline in pressure the maximum density has decreased to $\sim$ 5200 cm^{-3}. The shock causes an increase in free electrons, which catalyse the formation of H_2. Hence, this increase in the dominant coolant allows the low density shocked gas to cool down to the CMB temperature (i.e. 30 K). The clump reaches its maximum density of $\sim$ 78000 cm^{-3} around 0.47 Myrs after the initial blast wave and, although the minimum temperature within the lower density region of the clump is 30K, the temperature of the maximum density region is $\sim$300 K (Figure 4). During the shock-cloud interaction, the clump mass has increased from 19 $M_\odot$ to 40 $M_\odot$. We do not expect this clump to be gravitationally unstable as the minimum Jeans mass is 1000 $M_\odot$ (Figure 4).

After the passage of the shock the dense cloud is embedded in the high pressure, hot, low density interior of the supernova remnant. Our simulations do not have the spatial resolution to resolve the boundary layer between these two phases (we also do not include thermal conduction or model the external irradiation of the cloud), so the details of the boundary layer are probably not very reliable. The dominant physical process, however, is the simple pressure confinement of the cloud, and this is well-captured by our calculation. By the time the cloud is accelerated off the simulation domain it is entering an equilibrium phase of a pressure-confined cloud, similar to the cometary phase for irradiated clouds (Bertoldi & McKee 1990).

4 DISCUSSION

We have modelled a metal-free environment at redshift $z = 10$, which is associated with a protogalaxy formed from pristine primordial gas. We would expect hyper metal poor stars such as SDSS J102915+172927 (with a total metallicity $Z < 10^{-5} Z_\odot$) to have formed in a similar environment. To establish if it is possible to form low-mass stars we include non-equilibrium chemistry to capture the radiative cooling that would take place the interaction of a shock and a small cloud. We have included a metal-free chemistry to model this interaction. This may be a simplification when modelling supernovae, as the metals from the ejecta would interact and mix within the shell when the discontinuity between the shell and the supernova ejecta is being disrupted by the interaction with the clump (Tenorio-Tagle 1996). We would expect the metallicity of the shell to be near zero (Salvaterra et al. 2004) and according to Cen & Riquelme (2008) the shock velocity ensures that the clump remains mostly unaffected by metals. If this is true then modelling the shock and cloud as metal-free is a good approximation, as including metal-diffusion is beyond the scope of this work.

Within our Galaxy it is observed that if a blast wave from a supernova collides with the shell created by the progenitor's H II region and begins to travel within a neutral multi-phase medium (Reach et al. 2005). Although there is a lack of efficient coolants available in metal-free gas compared to the Galactic environment, we still expect density perturbations and therefore clumping to occur. As molecular hydrogen is the most efficient coolant available, the clump only has an initial density enhancement of 10 compared to the ambient medium. Hence the idealised case of a single density interstellar medium utilised in some supernova models may not reflect the true nature of the environment. Just increasing the ambient density from 1 cm^{-3} to 2 cm^{-3} causes the shell to develop much quicker and a larger shell travels slower by the time it reaches the clump. There is also a difference in pressure of a supernova shell sweeping into a hot ionised gas and when it sweeps colder neutral gas. All these factors need to be taken into account, which entails modelling the H II region prior to the supernova explosion, as we have done. The parameter space of ambient densities should be explored further in future work.

We assume that the progenitor star is formed in a dark matter halo that is large enough so that edge effects do not need to be taken into account for a radius of $r \leqslant 50$ pc. Vasiliev et al. (2008) highlighted an important link between the radial distribution of primordial gas prior to the supernova explosion and the subsequent evolution of the supernova remnant; and the state of the supernova shell is directly influences the formation of extremely metal-poor stars. This distribution is heavily dependent on the size of the metal-free star and its H II region prior to the explosion. Studies which reproduce the abundance patterns in extremely metal poor stars by modelling the evolution and explosion of metal-free stars stars and then comparing yields to observations (Nomoto et al. 2006; Joggerst et al. 2009, 2010), suggest that these stars are formed by metal-free stars within a mass range of $15 - 40$ $M_\odot$. The explosion mechanism for metal-free stars is uncertain, especially above 30 $M_\odot$, and so the star can have a range of explosion energies from $0.6 - 10 \times 10^{51}$ erg, which are associated with core collapse supernovae and hypernovae. The star is in this model is assumed to have an initial mass of 40 $M_\odot$.

A clump initially at distance $r \geqslant 40$ pc from the star can safely be assume to be neutral, because Figure 1 shows that the clump does not interact with any ionising radiation. Clouds found closer to the progenitor star may evaporate, or at a minimum, have a different thermal state to a neutral cloud. Radiation within the between $11.18 - 13.6$ eV photodissociates H_2 molecules and so has a knock-on heating effect on the gas. This dissociation radiation propagates further than ionising radiation, and without any dust present we expect that clump is completely atomic in the pre-supernova stage. In the 2D model dissociative photons from the hot gas is assumed to be negligible (Vasiliev et al. 2008), but the possi-

Model No.	Supernova Energy (10^{51} erg)	Ambient cloud density (cm^{-3})	H II region included	Clump density (cm^{-3})	Temperature of clump (K)	Clump distance (pc)	Shock velocity (km s^{-1})	Clump fate
M01	10	10	Yes	100	872	46	39	compressed clump
M02	2.0	10	Yes	100	872	46	-	shell stalled
M03	1.0	10	Yes	100	872	46	-	shell stalled
M04	0.6	10	Yes	100	872	46	-	shell stalled
M05	10	1	No	100	200	50	200	destroyed
M06	2.0	1	No	100	200	50	46	small fragments
M07	1.0	1	No	100	200	50	26	destroyed
M08	0.6	1	No	100	200	50	16	destroyed
M09	1.0	1	No	100	200	40	49	small fragments

Table 2. This table presents the initial conditions of a number of shock-cloud models and the corresponding fate of the clump at the end of the simulation. There are four end states of the clump: i) the clump is unaffected by the shock as the shell stalled before reaching the clump, ii) the clump is fully compressed into a single core, iii) the clump fragments into smaller dense pieces and iv) the clump no longer exists and is destroyed.

ble effects of UV radiation on the clump should be investigated in more detail in future work.

After exploring a number of explosion energies (see models M01−M04 in Table 2), we found that only the shock formed from a hypernova explosion (10^{52} erg) reached and compressed the clump. When extending our study by exploring other ambient cloud densities (models M05−M09 in Table 2), it emerges that the shock velocity determines the fate of the neutral clump. If the shock is too fast the clump is destroyed. When the supernova shock is too slow, the clump is only slightly compressed by inevitably destroyed. This is because the initial shock causes a secondary shock to travel through the rest of the clump, finally the gas disperses and flows downstream with the supernova shock. We therefore find that a small range of shock velocities ($30-50$ km s^{-1}) which can cause the clump to compress or fragment. Here the cooling time is equal to or less than the collapse/compression time and the velocity of the shock causes at least half of the clump to be compressed. Shock velocities above 40 km s^{-1}, cause the clump to fragment into smaller clumps, while below this velocity we find the clump is compressed.

The clump is near a supernova remnant so it will be exposed to cosmic rays, but the cosmic ray spectrum and intensity is unknown because of uncertainties in the expected interstellar magnetic field and the explosion mechanism for metal-free stars. We have assumed that the spectrum with be close to the observed spectrum in the Galactic environment, in keeping with Stacy & Bromm (2007). The effects of a range of cosmic ray ionisation rates ($10^{-18}-10^{-15}$ s^{-1}) and their associated heating on the shock-clump interactions will be explored in a future paper. In this model we include a background cosmic ray ionisation rate of 10^{-18} s^{-1}, as this rate was found to produce an overall cooling effect. As the clump is ~ 45 pc from the supernova explosion site, it is unlikely to be exposed to a high cosmic ray ionisation rate. We have not explored X-rays in this work, which would be produced by the supernova remnant. This would increase the H_2 abundance of gas ahead of the shell by increase the free electron content (Ferrara 1998; Haiman et al. 1997) and should be subject to further investigation.

The shocked clump of model M01 implodes because of the passage of the supernova shock (Figure 3). This is the same behaviour seen in 3D simulations of clouds interacting with clumps (Melioli et al. 2006; Leão et al. 2009; Johansson & Ziegler 2013), and earlier 2D work (e.g. Klein et al. 1994). We find that in our simulation the clump gains a maximum density of ~ 78000 cm^{-3}, which is a density enhancement of $10^{2.89}$ but does not become Jeans unstable. Vaidya et al. (2013) show that self-gravity has no effect on the clump at this point of the shock interaction, where the implosion is presssure-driven and the clump reaches its maximum density. However, self-gravity can become important at later stages when the clump relaxes. This gives us confidence that the implosion phase is correctly captured by our simulation. Johansson & Ziegler (2013) investigate the compression of a $n = 17\,\mathrm{cm}^{-3}$ cloud (with radius 1.5 pc) including a weak initial magnetic field and find higher densities enhancements of $10^3 - 10^5$. They also conclude that the clump will not become Jeans unstable. It is worth noting that their work considers solar metallicity gas with an equilibrium cooling function. Hence this may change when the model is refined to include non-equilibrium cooling.

Dust is assumed to be the major coolant in low-metallicity environments (Klessen et al. 2012; Schneider et al. 2012). How quickly it can form in a primordial supernova ejecta and the extent of mixing that would occur during this cloud-shock interaction are still open questions. It is believed that dust is quickly destroyed in the reverse shocks formed when the supernova shell begins to travel within the multiphase neutral medium (Cherchneff & Dwek 2010; Silvia et al. 2010). Without much dust in the environment, we cannot expect metal-line cooling to drastically lower the Jean mass, especially at metallicities $\leqslant 10^{-5}\,Z_{\odot}$. In light of this, much further work is required to investigate the effects of cosmic rays and external radiation fields (especially X-ray and UV) on this process, because there may be important positive feedback effects (Ricotti et al. 2002; O'Shea et al. 2005) that have not been considered so far.

5 CONCLUSION

We have presented a metal-free shock-cloud model, which simulates a supernova remnant interacting with a cloud at redshift $z = 10$. We model a dense clump ($n = 100$ cm^{-3}, $r = 1.3$ pc) embedded in a 10 cm^{-3} ambient cloud, which is 40 pc from the progenitor star. We consider realistic pre-supernova conditions by including the effects of stellar radiation from a 40 $M_{\odot}$ metal-free star on the multi-phase neutral medium. At the end of the star's main-sequence lifetime, a hypernova (10^{52} erg) is initiated and the evolution of the supernova shell and its subsequent interaction with the dense clump is studied. Radiative cooling is a crucial process in the shock-cloud interaction, allowing the formation of dense cold gas that may be susceptible to gravitational collapse. During this process we have comprehensively modelled the radiative (non-equilibirum) cooling taking place.

We followed the evolution of the supernova remnant and its interaction with the surrounding ionised and neutral medium. When

the radiative shell interacts with the metal-free clump, it reaches a maximum of density $\sim$ 78000 cm^{-3}. This is a $10^{2.89}$ density enhancement and is consistent with Galactic shock-cloud models considering solar metallicity gas with equilibrium cooling functions. The clump undergoes a reduction in Jeans mass from 10^5 M$_\odot$ to 10^3 M$_\odot$, but does not become gravitationally unstable. Further work is required to ascertain the effect of cosmic rays, X-rays and UV radiation on the clump during the supernova phase.

In this work, we found an optimal range of shock velocities ($30 - 50$ km s^{-1}) which compress small metal-free clouds. Below this range the cloud is slightly perturbed by the supernova shock and is not subject to any appreciable density enhancement. Above this range the clumps are destroyed, therefore the results by Mackey et al. (2003) are overoptimistic, as they assume the cloud survives a 200 km s^{-1} interaction. The shock is in its radiative phase when it collides with the dense clump. Hydrodynamic instabilities are likely to be more important than gravity in radiative supernova shells Vishniac (1983), especially once the shell has encountered neutral matter, hence 1D models (without metal diffusion) may not be adequate to study the formation of the second generation of stars. Consequently it is still an open question where these hyper metal poor stars form.

When investigating model M01, we have achieved an appreciable Jean mass reduction of a small dense clump and a density enhancement comparable to Galactic studies, by including non-equilibrium metal-free radiative cooling. Further refinement of this model by including low-metallicity chemistry and thermal models plus positive feedback effects from cosmic rays, X-rays and UV radiation, may cause a further reduction in Jeans mass. From this work we recognise that non-equilbrium cooling is dominant process in shock-cloud interactions, and that Galactic studies would benefit by extending present models that utilise cooling curves which assume collisional ionisation equilibrium.

ACKNOWLEDGEMENTS

The authors would like to thank S.C.O. Glover and J.M.C. Rawlings for their helpful discussions. This work used the DiRAC Complexity system, operated by the University of Leicester IT Services, which forms part of the STFC DiRAC HPC Facility (www.dirac.ac.uk). This equipment is funded by BIS National E-Infrastructure capital grant ST/K000373/1 and STFC DiRAC Operations grant ST/K0003259/1. DiRAC is part of the National E-Infrastructure. JM acknowledges funding during this project by a fellowship from the Alexander von Humboldt Foundation and from the Deutsche Forschungsgemeinschaft priority program 1573, "Physics of the Interstellar Medium".

REFERENCES

Bertoldi F., McKee C. F., 1990, ApJ, 354, 529
Caffau E., Bonifacio P., Franc cois P., Sbordone L., Monaco L., Spite M., Spite F., Ludwig H.-G., Cayrel R., Zaggia S., Hammer F., Randich S., Molaro P., Hill V., 2011, Nature, 477, 67
Cen R., Riquelme M. A., 2008, ApJ, 674, 644
Cherchneff I., Dwek E., 2010, ApJ, 713, 1
Chiaki G., Yoshida N., Kitayama T., 2013, ApJ, 762, 50
Falle S. A. E. G., 1991, MNRAS, 250, 581
Ferrara A., 1998, ApJ, 499, L17
Fukugita M., Kawasaki M., 1994, MNRAS, 269, 563
Galli D., Palla F., 1998, A&A, 335, 403
Glover S. C. O., Abel T., 2008, MNRAS, 388, 1627
Glover S. C. O., Jappsen A.-K., 2007, ApJ, 666, 1
Glover S. C. O., Savin D. W., 2009, MNRAS, 393, 911
Haiman Z., Rees M. J., Loeb A., 1997, ApJ, 476, 458
Hollenbach D., McKee C. F., 1979, ApJS, 41, 555
Hummer D. G., 1994, MNRAS, 268, 109
Iliev I. T., Ciardi B., Alvarez M. A., Maselli A., Ferrara A., Gnedin N. Y., Mellema G., Nakamoto T., Norman M. L., Razoumov A. O., Rijkhorst E.-J., Ritzerveld J., Shapiro P. R., Susa H., Umemura M., Whalen D. J., 2006, MNRAS, 371, 1057
Joggerst C. C., Almgren A., Bell J., Heger A., Whalen D., Woosley S. E., 2010, ApJ, 709, 11
Joggerst C. C., Woosley S. E., Heger A., 2009, ApJ, 693, 1780
Johansson E. P. G., Ziegler U., 2013, ApJ, 766, 45
Jun B.-I., Jones T. W., Norman M. L., 1996, ApJ, 468, L59
Kitayama T., Yoshida N., 2005, ApJ, 630, 675
Klein R. I., McKee C. F., Colella P., 1994, ApJ, 420, 213
Klessen R. S., Glover S. C. O., Clark P. C., 2012, MNRAS, 421, 3217
Leão M. R. M., de Gouveia Dal Pino E. M., Falceta-Gonçalves D., Melioli C., Geraissate F. G., 2009, MNRAS, 394, 157
Machida M. N., Tomisaka K., Nakamura F., Fujimoto M. Y., 2005, ApJ, 622, 39
Mackey J., 2012, A&A, 539, A147
Mackey J., Bromm V., Hernquist L., 2003, ApJ, 586, 1
Mackey J., Lim A. J., 2010, MNRAS, 403, 714
Mackey J., Lim A. J., 2011, MNRAS, 412, 2079
Melioli C., de Gouveia Dal Pino E. M., de La Reza R., Raga A., 2006, MNRAS, 373, 811
Nagakura T., Hosokawa T., Omukai K., 2009, MNRAS, 399, 2183
Nomoto K., Tominaga N., Umeda H., Kobayashi C., Maeda K., 2006, Nuclear Physics A, 777, 424
O'Shea B. W., Abel T., Whalen D., Norman M. L., 2005, ApJ, 628, L5
Peebles P. J. E., 1971, Physical cosmology
Raga A. C., Cantó J., Rodríguez L. F., Velázquez P. F., 2012, MNRAS, 424, 2522
Reach W. T., Rho J., Jarrett T. H., 2005, ApJ, 618, 297
Ricotti M., Gnedin N. Y., Shull J. M., 2002, ApJ, 575, 49
Salvaterra R., Ferrara A., Schneider R., 2004, New Astronomy, 10, 113
Sánchez-Salcedo F. J., Vázquez-Semadeni E., Gazol A., 2002, ApJ, 577, 768
Schaerer D., 2002, A&A, 382, 28
Schneider R., Omukai K., Limongi M., Ferrara A., Salvaterra R., Chieffi A., Bianchi S., 2012, MNRAS, 423, L60
Shapiro P. R., Kang H., 1987, ApJ, 318, 32
Silvia D. W., Smith B. D., Shull J. M., 2010, ApJ, 715, 1575
Slyz A. D., Devriendt J. E. G., Bryan G., Silk J., 2005, MNRAS, 356, 737
Stacy A., Bromm V., 2007, MNRAS, 382, 229
Sutherland R. S., Dopita M. A., 1993, ApJS, 88, 253
Tenorio-Tagle G., 1996, AJ, 111, 1641
Vaidya B., Hartquist T. W., Falle S. A. E. G., 2013, MNRAS, 433, 1258
Vasiliev E. O., Vorobyov E. I., Shchekinov Y. A., 2008, A&A, 489, 505
Verner D. A., Ferland G. J., 1996, ApJS, 103, 467
Vishniac E. T., 1983, ApJ, 274, 152
Voronov G. S., 1997, Atomic Data and Nuclear Data Tables, 65, 1

Woodall J., Agúndez M., Markwick-Kemper A. J., Millar T. J., 2007, A&A, 466, 1197

APPENDIX A: 1D SUPERNOVA SHELL EXPANSION

Fig. A1 shows the results of a 1D test, in which the expansion of a blastwave is followed using different chemistry/cooling assumptions: adiabatic with no chemistry, including chemistry but only atomic coolants, and including chemisty with atomic and molecular coolants. The radius of the SN forward shock (upper panel) and maximum density in the shell (lower panel) are plotted as a function of time since explosion. We used uniform radial grid with 5120 grid zones between $r = 0$ and $r = 130\,\mathrm{pc}$, and input 10^{51} ergs of thermal energy in the 8 grid zones closest to the origin. The ISM is a constant density medium with $\rho = 2.44 \times 10^{-24}\,\mathrm{g\,cm^{-3}}$ at a redshift of 20. The initial ISM temperature is $T = 10^4\,\mathrm{K}$ (corresponding to a pressure of $p \approx 1.5 \times 10^{-12}\,\mathrm{dyne\,cm^{-2}}$). Without any cooling this can be compared to the Sedov-Taylor solution, and when cooling and chemistry are included we compare to the results of Machida et al. (2005).

The adiabatic calculation matches the Sedov-Taylor solution until about 0.8 Myr, after which the shock runs ahead of this solution. The explanation for this is that the shock weakens as it slows down at late times, and the ISM ambient pressure is no longer negligible. This breaks the scale-free nature of the analytic solution, and the result is that the shock radius advances faster than predicted at late times (cf. Raga et al. 2012).

At about 0.05 Myr the simulations with cooling start to decelerate and deviate from the adiabatic solution. The expansion rate changes from the Sedov-Taylor value $R_{\rm sh} \propto t^{2/5}$ to the momentum-conserving value $R_{\rm sh} \propto t^{1/4}$. Atomic cooling is initially much stronger than molecular cooling, so both of these runs match each other until the molecular cooling begins to affect the shell and the ISM at $t \approx 0.2\,\mathrm{Myr}$. At later times the shell density in the cooling model decreases steadily because it can no longer cool, and the weak forward shock keeps adding lower entropy gas to the shell. The molecular cooling model has a higher density shell once molecular cooling becomes important at $t \approx 0.2\,\mathrm{Myr}$, because it can cool to much lower temperatures. This has the further effect that the shell remains at a high density for much longer.

The molecular cooling calculation shows that we get compression factors of $> 100\times$ in the shell at $t \geqslant 0.2\,\mathrm{Myr}$. This model disagrees strongly with Machida et al. (2005) (see their fig. 4), who found only weak density increase in the supernova shell for times up to 10^7 years. The density in their analytic model was set by the imposed pressure-confining boundary conditions on the shell, so we suspect that one of the boundary conditions was incorrect.

APPENDIX B: CHEMISTRY NETWORK

The full chemical network is displayed in Table B1. All the molecular reaction rates (R07 -R42) have been adapted for the temperature range ($10 - 10^9$ K) have been divided into two categories: i) Formation rates (listed in Table B2) and ii) Destruction rates (listed in Table B3).

Most of the UMIST 06 rates are valid until 41,000K. If a formation rate is valid up to a lower temperature, the value at the maximum temperature range is kept constant for temperatures above until 41,000K. Above 41,000 K all formation rates are cut-offand the reaction rates take on the the following forms:

$$K_1 = k \times \exp\left(1.0 - \frac{\mathrm{T}}{41000.0}\right)$$

$$K_2 = k \times \exp\left(10 \times \left(1.0 - \frac{\mathrm{T}}{41000.0}\right)\right)$$

where k is the value of the rate at 41000K. The details of how each formation reaction is treated, can be found in Table B2.

The destruction rates are extrapolated above their valid temperature range. Above this temperature, if there is a maximum value after which the rate decreases (T_{ex}), this maximum value is kept constant for all higher temperatures ($\mathrm{T} > \mathrm{T}_{ex}$). All the destruction rates, with the corresponding maximum extrapolation temperatures and temperatures ranges are displayed in Table B3.

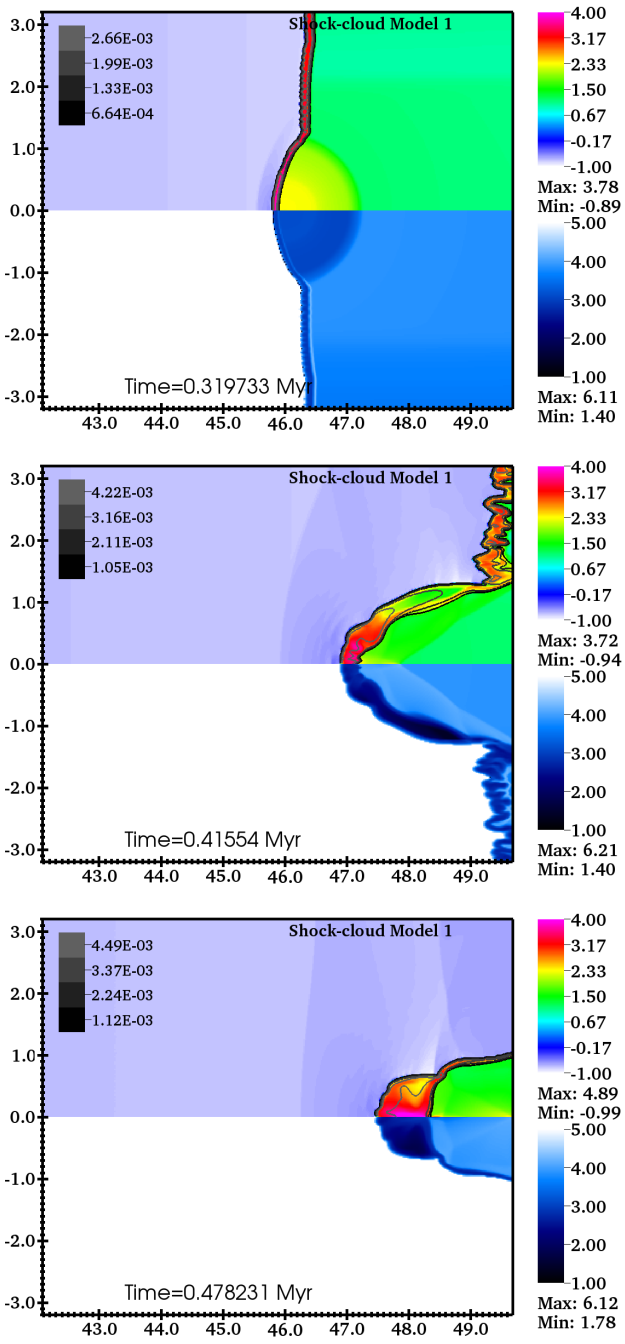

Figure 3. Log of H number density ($\log_{10}(n_{\rm H}/{\rm cm}^{-3})$, colour scale) is plotted on the upper half-plane, and Log of temperature on the lower half-plane (blue scale), with linearly-spaced H_2 fraction contours overplotted on the upper half-plane, for an early time as the cloud is being shocked (top), while the shock has passed through the cloud (centre) and after the cloud has been compressed and accelerated by the shock (below). The x-axis shows distance from the star in parsecs, and the y-axis shows radial distance from the axis of symmetry of the 2D calculations (the lower half-plane is a reflection of the simulation domain to negative values).

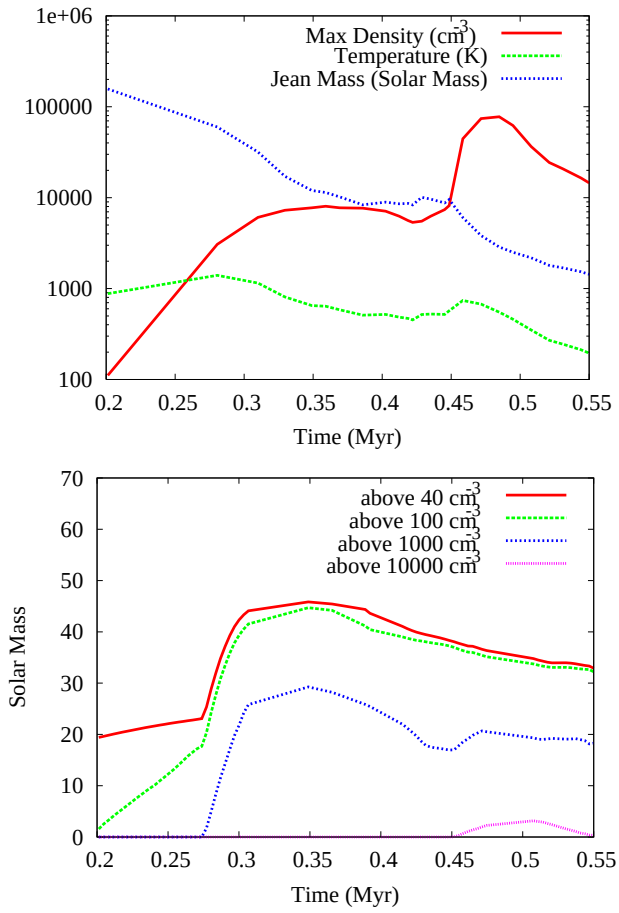

Figure 4. The upper plot displays the maximum density of within the clump as the shock passes through, along with the temperature of the maximum density point and associated Jeans mass. The lower plot displays the mass within the clump as a function of different densities.

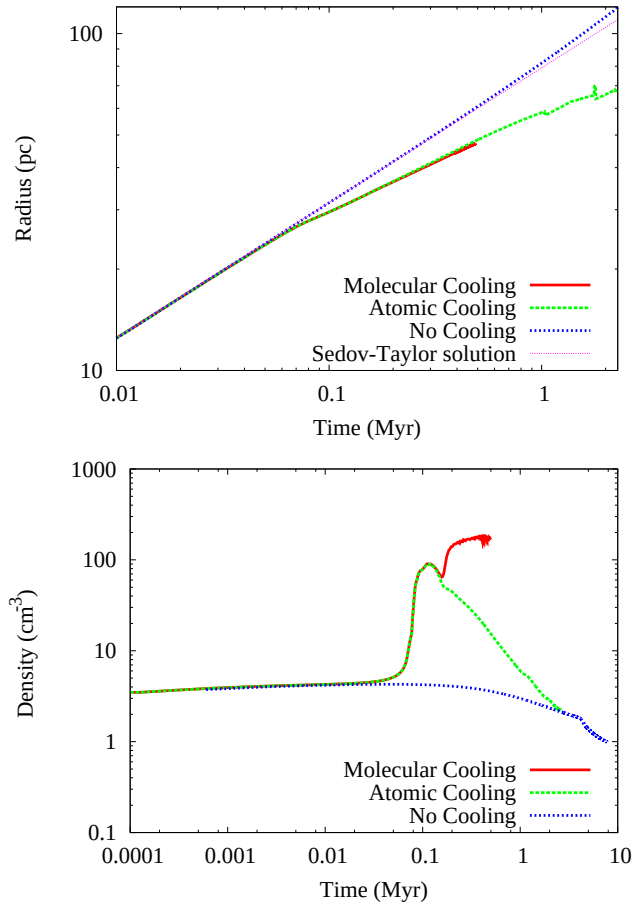

Figure A1. Supernova shell expansion as a function of time for an adiabatic calculation, a calculation with atomic line cooling only, and a calculation with atomic and molecular cooling switched on. The expansion radius is compared to the analytic Sedov-Taylor solution in the upper plot. The lower plot shows the maximum gas number density in the shell as a function of time for the same three models.

Reaction No.	Reaction	References for rate coefficients
R01	$H^+ + e^- \rightarrow H + \gamma$	H
R02	$He^+ + e^- \rightarrow He + \gamma$	VF
R03	$He^{++} + e^- \rightarrow He^+ + \gamma$	VF
R04	$H + e^- \rightarrow H^+ + e^- + e^-$	V
R05	$He + e^- \rightarrow He^+ + e^- + e^-$	V
R06	$He^+ + e^- \rightarrow He^{++} + e^- + e^-$	V
R07	$H_2 + H \rightarrow H + H + H$	GA08
R08	$H^- + H \rightarrow H + H + e^-$	GA08
R09	$H^- + He \rightarrow He + H + e^-$	GA08
R10	$H_2 + H_2 \rightarrow H_2 + H + H$	UM06
R11	$H^- + e^- \rightarrow H + e^- + e^-$	JR
R12	$H_2 + He^+ \rightarrow He + H^+ + H$	UMO6
R13	$H_2 + e^- \rightarrow H + e^- + H$	UM06
R14	$H_2^+ + e^- \rightarrow H^+ + e^- + H$	R14*
R15	$HeH^+ + e^- \rightarrow He^+ + e^- + H$	R14*
R16	$H^+ + H \rightarrow H_2^+ + \gamma$	UM06, GA08
R17	$H^+ + He \rightarrow HeH^+ + \gamma$	UM06
R18	$H + e^- \rightarrow H^- + \gamma$	UM06, GA08
R19	$HeH^+ + e^- \rightarrow He + H$	UM06
R20	$H_2^+ + e^- \rightarrow H + H$	UM06
R21	$H_3^+ + e^- \rightarrow H + H + H$	UM06
R22	$H_3^+ + e^- \rightarrow H_2 + H$	UM06
R23	$H^- + H_2^+ \rightarrow H + H + H$	GA08
R24	$H + He^+ \rightarrow He + H^+$	UM06,hd
R25	$H_2 + He^+ \rightarrow He + H_2^+$	UM06
R26	$H^+ + H^- \rightarrow H + H$	UM06
R27	$H^- + H_2^+ \rightarrow H_2 + H$	UM06
R28	$H^- + He^+ \rightarrow He + H$	UM06
R29	$H + H_2^+ \rightarrow H_2 + H^+$	UM06
R30	$H_2^+ + H_2 \rightarrow H_3^+ + H$	UM06
R31	$H^- + H_3^+ \rightarrow H_2 + H_2$	UM06
R32	$H + HeH^+ \rightarrow He + H_2^+$	UM06
R33	$H_2 + HeH^+ \rightarrow He + H_3^+$	UM06
R34	$H_2^+ + He \rightarrow HeH^+ + H$	UM06
R35	$H^- + H^+ \rightarrow H_2^+ + e^-$	SK87
R36	$H^- + H \rightarrow H_2 + e^-$	UM06
R37	$H + CR \rightarrow H^+ + e^-$	UM06
R38	$He + CR \rightarrow He^+ + e^-$	UM06
R39	$H_2 + CR \rightarrow H^+ + H + e^-$	UM06
R40	$H_2 + CR \rightarrow H + H$	UM06
R41	$H_2 + CR \rightarrow H^+ + H^-$	UM06
R42	$H_2 + CR \rightarrow H_2^+ + e^-$	UM06

Table B1: Metal free chemistry network:
References- UM06 =UMIST database for astrochemistry [rate 06, non-dipole enhanced] (Woodall et al. 2007); GA08 = Glover & Abel (2008); H =Hummer (1994); GP98 = Galli & Palla (1998); SK87= Shapiro & Kang (1987); hd = matching scheme; R14*= same value as R14; JR= private communication with Jonathan Rawlings; V=Voronov (1997); VF= Verner & Ferland (1996)

Reaction Number	Valid Temperature Range (K)	Below Minimum Temperature	Above Maximum Temperature	Cut off Type T >41000K
R16	S:10 – 32000	-	C	CT2
R17	16 – 100	C	E	CT
R18	S:10 – 41000	-	-	CT2
R29	10 – 41000	-	-	CT
R30	10 – 41000	-	-	CT
R33	10 – 41000	-	-	CT
R34	10 – 41000	-	-	CT
R35	10 – 41000	-	-	CT
R36	S:10 – 41000	-	-	CT

Table B2. Molecular reactions that are cut-off at 41000 K: E= rate extrapolated; C= max/min value kept constant and extended; - = Not Applicable; S= switching between different reaction rates within temperature range; CT2= $k \exp(10.0 \times (1.0 - \mathrm{T}/41000))$ and CT= $k \exp(1.0 - \mathrm{T}/41000)$ are exponential cut-off for T> 41000K and k is the value of the reaction rate at 41000 K

Reaction Number	Valid Temperature Range of Rate (K)	Below Range	Above Range	Maximum Extrapolation Temperature T_{ex} (K)
R07	1833 – 41000	E	E	10^9
R08	10 – 10000	-	C	-
R09	10 – 10000	-	C	-
R10	2803 – 41000	E	E	10^7
R11	10 – 41000	-	E	10^5
R12	100 – 300	E	E	10^8
R13	3400 –41000	E	E	10^8
R14	3400 –41000	E	E	10^8
R15	3400 –41000	E	E	10^8
R19	10 – 300	-	E	10^9
R20	10 – 300	-	E	10^9
R21	10 – 1000	-	E	10^9
R22	10 – 1000	-	E	10^9
R23	10 – 10000	-	C	-
R24	S:10 – 41000	-	C	-
R25	10 – 300	-	E	10^9
R26	10 – 300	-	E	10^4
R27	10 – 300	-	E	10^9
R28	10 – 300	-	E	10^9
R31	10 – 300	-	E	10^9
R32	10 – 41000	-	E	10^9
R37	10 – 41000	-	C	-
R38	10 – 41000	-	C	-
R39	10 – 41000	-	C	-
R40	10 – 41000	-	C	-
R41	10 – 41000	-	C	-
R42	10 – 41000	-	C	-

Table B3. Molecular reactions adapted to maximum temperature (10^9 K): E= rate is extrapolated to a maximum Extrapolation Temperature (T_{ex}) and then extended as a constant after that temperature; C= max/min value kept constant; - = Not Applicable; S= a number of reaction rates utilised within temperature range